Catalysis Today 442 (2024) 114911

Contents lists available at ScienceDirect

Catalysis Today

journal homepage: www.elsevier.com/locate/cattod

Vanadium-containing modified clays as catalysts for acetaldehyde production by ethanol selective oxidation

Ema V. Sabre [a,b], Sandra G. Casuscelli [a], Analía L. Cánepa [a], Vicente Cortés Corberán [b,*]

[a] Centro de Investigación y Tecnología Química, CITeQ-UTN-CONICET, Facultad Regional Córdoba, Maestro López esq. Cruz Roja Argentina, s/n, Córdoba X5016ZAA, Argentina

[b] Institute of Catalysis and Petroleumchemistry (ICP), Spanish Council for Scientific Research (CSIC), Marie Curie, 2, Madrid 28049, Spain

ARTICLE INFO

Keywords:
Titanium modified clay
Supported vanadium catalysts
Selective oxidation
Ethanol oxidation
Acetaldehyde production
Sustainable raw materials

ABSTRACT

This work investigates use of natural clays as a sustainable raw material to prepare supported vanadium catalysts for the aerobic selective oxidation of ethanol to produce acetaldehyde. As dispersion and nature of the supported V species depend on its interaction with the support surface and its specific surface area, montmorillonite extracted from an Argentinian bentonite clay was pillared with titania, and vanadium was added by wet impregnation to get V/Ti-PILC catalysts. The effects of catalyst V content (0.5 – 2 wt%), reaction temperature (250 – 350 ºC) and O_2/ethanol molar ratio (0.5 – 1.5) on their performance for this reaction were studied. Characterization by X-ray diffraction (XRD) and N_2 adsorption/desorption isotherms showed that the synthesized catalysts maintained the mesoporous structure after the V addition, though their lamellar structure lost regularity. Under the reaction conditions explored, all the V/Ti-PILC catalysts were active and very selective to acetaldehyde (80 %), their activity increasing with V content. The highest activity was associated with the highest dispersion of isolated tetrahedral vanadium centers, identified by diffuse reflectance UV-Vis, Raman and X-ray photoelectron (XPS) spectroscopies. The highest ethanol conversion (87 %), with 85 % selectivity to acetaldehyde, was reached over the catalyst with 2 wt% of V at 350 ºC with O_2/ethanol = 1. The acetaldehyde yield and selectivity values reached are comparable with those reported for related mesoporous catalysts, which allows to consider these supports a sustainable alternative for high surface area supported vanadium catalysts.

1. Introduction

Selective oxidation is one of the most important reactions in industrial chemical processes. Notably, selective oxidation of alcohols to carbonyl compounds is interesting in synthetic organic chemistry because the products obtained can be used as precursors and/or intermediates to obtain drugs, vitamins and fragrances [1–4]. In addition, alcohols are attractive as raw material because can be obtained from renewable resources instead of fossil reserves [5]. Bioethanol can be produced from biomass fermentation using agricultural and forestry resources and residues, contributing to the Bio-Circular-Green (BCG) economy, since it recovers residues and converts them into high value bio-based chemicals [6].

Acetaldehyde (AcH) is an industrially important solvent and intermediate for the production of a wide range of organic compounds (acetic acid, ethyl acetate, pentaerythritol, crotonaldehyde, pyridine derivatives, etc.) used in chemical synthesis, pharma, food paper, plastics and paints sectors. Acetaldehyde market demand was roughly 1.14 million tons in 2022 and with an estimated CAGR of 4.50 % until 2032 [7]. However, currently around 85 % of AcH is produced from ethylene from fossil resources via the liquid phase Wacker-Hoechst process catalyzed by $PdCl_2$-$CuCl_2$ [8]. An alternative is the catalytic gas-phase oxidation of ethanol (EtOH) by molecular oxygen (from air) because it is an economic and more environmentally friendly process. Copper, silver, and their oxides or alloys are the most frequently used catalysts for this in the industry. For instance, the Veba-Chemie Process uses a silver catalyst operating at 500 – 650 ºC [9]. Thus, the development of a more effective and sustainable gas phase process is a challenge for chemical industry.

Vanadium oxide catalysts are effective in oxidehydrogenation (ODH) and selective oxidation of a range of organic compounds, such as alkanes [10], aromatics [11] and alcohols [12]. Though bulk vanadia catalyzes the total oxidation, highly dispersed vanadium oxide species (isolated V atoms, oligomers or monolayers) are selective to dehydrogenated or

* Corresponding author.
E-mail address: vcortes@icp.csic.es (V. Cortés Corberán).

https://doi.org/10.1016/j.cattod.2024.114911
Received 4 February 2024; Received in revised form 4 June 2024; Accepted 24 June 2024
Available online 26 June 2024

partially oxidized products [10,13]. This implies a significant influence of nature and dispersion of V species on the catalytic efficiency [13–17]. Thus, efforts have been devoted to increase such dispersion by improving the interaction with the support (for instance, by using the surface of bulk [13] or supported titania [12] to get it) or by using high specific surface area supports to increase the vanadium load while keeping good dispersion.

Different V-modified mesoporous materials, with specific areas between 170 and 1100 m^2/g, have been evaluated in EtOH oxidation [18–21]. Cánepa et al. [20] reported that dispersion of isolated tetrahedral vanadium centers in V-MCM-41 catalysts are responsible for obtaining the best catalytic performance in EtOH oxidation (AcH selectivity up to 90.5 % and yield up to 48 % were reached using the most active catalyst). Although all catalysts showed similar specific areas, around 1100 m^2/g, increasing the V content produces the polymerization of V species forming clusters $(V^{\delta+}\ldots O^{\delta-}\ldots V^{\delta+})_n$, so an important part of the V is not accessible to the reactants. Autthanit et al. [21] investigated the catalytic performance of different VOx/SBA-15 catalysts for EtOH non-oxidative and oxidative dehydrogenation (80 % EtOH conversion and 48 % AcH selectivity in non-oxidative dehydrogenation and 98 % EtOH conversion and 41 % AcH selectivity in oxidative dehydrogenation). SBA-15 supports were synthesized using the sol-gel and hydrothermal methods, achieving a better vanadium dispersion and monomeric VO_X or VO_4^{3-} species by the hydrothermal method. Although these ordered mesoporous materials with high specific areas show good performance in EtOH oxidation, the V dispersion on them shows a practical limit of V loading, and their hydrothermal synthesis is expensive and environmentally unfriendly (solvents, surfactants, wastes, non-mild conditions, etc.).

Clay minerals can be an important alternative for generating sustainable mesoporous catalyst supports due to their low cost and abundance in nature and their properties, which allow structural, textural and chemical modifications [22]. Bentonite, a clay of the smectite group, consists of aluminum phyllosilicate. Its sheet laminar structure consists of a layer of octahedral alumina $[Al_2(OH)_6]$ between two layers of tetrahedral silicates $[SiO_4]^{4-}$ with charge-compensating cations between layers (generally Na^+, Ca^{2+} and Mg^{2+}). Besides, it contains montmorillonite, quartz, feldspar, volcanic glass, organic matter, gypsum or pyrite [23]. Their swelling capacity allows its modification through simple processes to become an appropriate material for catalytic applications. In this sense, pillaring process can modify their properties by exchanging the charge-compensating cations between clay layers with large inorganic cations, which are polymeric or oligomeric hydroxyl metal cations, formed by the hydrolysis of metal oxides or metal salts. Then, dehydration and dehydroxylation by heating forms stable metal oxides that act as pillars between the silicate layers creating interlayer spaces of molecular dimensions and increasing the porosity [23–26]. The materials obtained after pillaring process, identified as pillared clays (PILCs), possess arrangements of the laminar face-to-face type, where microporosity is predominant.

On the other hand, changes may occur in the structure of the pillared clays by modifying some parameters of the synthesis of these materials, such as the nature of the clay used as the starting material, nature of the metallic cation, hydrolysis conditions, reaction time, synthesis temperature, and the washing, drying and calcination processes [27–30]. For example, delaminated pillared clay is one class of pillared clay characterized by a house-of-card like structure (with edge-type or edge-side edge arrangements) containing mesopores and macropores, in addition to micropores found in pillared clays [31]. The different porosity characteristics of delaminated pillared clays compared to pillared clays will influence their catalytic and adsorption properties [32]. Consequently, bentonite clays modified by pillaring processes may be a promising alternative as supports to obtain efficient catalysts in alcohol oxidation reactions.

This context motivates us to investigate the use of modified bentonite as an easily available, sustainable high surface area support for vanadium catalysts for EtOH selective oxidation under mild reaction conditions. Thus, in this work we synthesized and characterized modified Ti-PILC with different V contents (0.5–2 wt%), using a titania precursor for the clay pillaring to favor vanadium dispersion. Their catalytic activity was investigated in EtOH selective oxidation with oxygen at different temperatures. In addition, the effect of feed composition was studied with the best performing catalyst. The acetaldehyde yield and selectivity values reached are comparable to those reported with other mesoporous vanadium catalysts.

2. Experimental

2.1. Catalyst synthesis

The supports were synthesized from a bentonite clay obtained in San Juan province, Argentina. The bentonite clay was firstly sieved to a size of 200 mesh and underwent several washing stages to remove undesired contaminants. Then it was mixed with water and the aqueous suspension was left to settling for a day to separate the fraction of larger particles, recovering the fraction of smaller particles including montmorillonite. Subsequently, the solid was separated by centrifugation and dried in the oven at 120 °C for 12 h. Then, this solid was mixed with 0.99 M NaCl solution to exchange its cations with Na^+. This suspension was stirred for 8 h at room temperature before the solid was separated by centrifugation and washed with distilled water until free of Cl^- ions. Finally, the solid was dried at room temperature and named as Na-mont. Then, Ti-PILC was synthesized from Na-mont by exchanging Na^+ ions with large hydroxyl polycations of Ti coming from pillaring solution. This solution was prepared by adding dropwise the necessary amount of Ti $(OC_4H_9)_4$ (Fluka) to a solution of 6.16 M HCl under vigorous stirring, to obtain a Ti/clay final ratio of 10 mmol/g. The exchange was produced by adding dropwise the aqueous suspension of 8.00 g/L Na-mont to the pillaring solution and then aging for 12 h under vigorous agitation. The solid fraction was separated by centrifugation, washed with distilled water until it was free of Cl^- ions, dried at room temperature and then calcined at 450 °C for 2 h. Subsequently, to obtain the catalysts, vanadium was incorporated into the Ti-PILC support by wet impregnation using an aqueous solution with the necessary amount of $VOSO_4.xH_2O$ (99 % Aldrich) to reach metal loadings between 0.5 and 2 wt%. The solvent was removed in a rotary evaporator and finally the dry solids were calcined at 450 °C for 3 h under air flow and named as xV/Ti-PILC, where x is the theoretical V loading expressed as wt%.

2.2. Catalyst characterization

XRD patterns were recorded in the 2θ angular range of 1 – 60º with an angular resolution of 0.02°, using a PANalytical XPert PRO diffractometer with a Cu Kα (λ = 1.5406 Å) radiation source. The XRD patterns were recorded at a scanning speed of 2º/min.

The specific surface, micropores and mesopores volume and pore diameter were determined from N_2 adsorption-desorption data obtained using a Micromeritics ASAP Instrument at −196 °C. Before the measurement the sample was degassed at 300 °C under vacuum for 5 hours. The specific surface was determined by the Brunauer-Emmett-Teller method (S_{BET}) and the pore size distributions were calculated using the NLDFT model for pillared clays.

The metal content in the solids was determined by Inductively Coupled Plasma Optical Emission Spectroscopy (ICP-OES), after digestion of the solids, using Agilent Technologies 5110 instrument.

Diffuse Reflectance UV–vis (DR-UV–vis) spectra were obtained with a Jasco V650 spectrometer between 200 and 800 nm and the data were converted employing the Kubelka-Munk equation.

X-ray photoelectron spectroscopy (XPS) analyses were performed on an ultra-high vacuum Thermo-Fisher Scientific K-Alpha X-ray photoelectron spectrometer system, equipped with a hemispherical energy analyzer and a monochromatic X-ray source was used for surveying the

photoemission spectra. The photoionization of the samples was induced by monochromatic Al Kα photons at 1486 eV. Binding energies of the chemical elements were corrected using the C 1 s photoemission signal at 284.8 eV as reference. The curve fitting was performed with Avantage software, using the Shirley baseline function and Gaussian - Lorentzian profile.

Raman spectra of the solids were registered at room temperature in a FT-Raman Bruker MultiRam equipment using an air-cooled diode pumped Nd:YAG laser, that emits at a wavelength of 1064 nm, as the excitation source. The scattered radiation was collected at 180° to the source, and spectra from 10 to 1100 cm^{-1} were recorded with a resolution of 4 cm^{-1} using 200 mW of laser power.

2.3. Catalytic activity

EtOH oxidation reaction tests were carried out between 250 and 350 ºC in a stainless steel, fixed-bed continuous flow reactor inside a Microactivity Reference (PID Eng & Tech) equipment. The catalyst particle size was previously selected (0.25–0.42 mm) based on tests to verify absence of diffusional control. A typical test used 0.08 g of catalyst diluted in SiC (catalyst/SiC = 1/3 v/v). The feed consisted in a mixture of EtOH, O_2 and He in the molar composition 7.1/x/(92.9-x) respectively, with a residence time W/F = 1.55 g cat.h/mol EtOH.

Quantification of reactants and products concentrations was carried out online by gas chromatography on a Varian Star 3400 CX instrument equipped with two packed columns, one filled with molecular sieve (for CO, O_2 and CH_4) and other with Porapak QS (for the rest of compounds), and a thermal conductivity detector. The yield of the products was calculated as a function of the carbon atoms and was defined as the ratio between the C atoms in the product and the C atoms of the fed EtOH. The sum of the yields of carbon products obtained was employed to calculate EtOH conversion. The mass balance in all tests was within 100 ± 5 %.

3. Results and discussion

3.1. Catalyst characterization

XRD patterns of clay minerals commonly present at low angle a basal reflection 001 considered as one of their main identification sources, attributed to the ordering of the layers and which allows to determine basal spacing (d_{001}) [33]. Fig. 1 shows low angle XRD patterns of Na-mont, Ti-PILC and 0.5V/Ti-PILC, where reflection (001) displays at 2θ = 7.2º for Na-mont with d_{001} ≈ 1.23 nm. In Ti-PILC pattern this reflection shifted towards to a lower value of 2θ (~ 1.3°) corresponding to d_{001} = 3.4 nm. This value is higher than the obtained for Na-mont and indicates the expansion of the layers due to pillars formation. However, the intensity of this reflection was very low compared to Na-mont, which would be associated with the formation of delaminated structure, characterized by non-parallel ordering of the clay layers [32,33]. In conclusion, a part of the oriented silicate layers exhibits the basal reflection, and the partially disordered structure by delamination could weaken the basal reflection as noted in the literature [34]. These results are in good agreement with those reported by Bergaya [35] who reported a d_{001} ≈ 3.0 nm for Ti-PILC, and in line with other authors: Yuan et al. [36,37] reported values of 6.64 nm and 6.54 nm for delaminated Ti-PILC and Fe-Ti-PILC, respectively, while Mandalia et al. [38] reported a d_{001} of 7.2 nm for Fe_2O_3-PILC. Therefore, long-range face-to-face arrangements characteristic of clays was distorted during the pillaring process promoting disordered house of cards structure. Modification of some synthesis parameters, such as aging time, nature of the clay and use of larger amounts of bentonite clays at the beginning of the synthesis, probably produced loss of regularity in the Ti-PILC laminated structure [32].

Instead, low angle XRD pattern of 0.5V/Ti-PILC (Fig. 1) does not show the (001) reflection. This reflection was absent in XRD patterns of all V-modified pillared samples (not shown here); so, XRD pattern of 0.5V/Ti-PILC is representative for the whole series. Other authors reported the absence of the (001) reflection and associated this to delamination of clays [26,29,39]. Taking into account that V was incorporated in Ti-PILC by wet impregnation, this absence can be associated to some stages of this process (such as the vigorous agitation used during the mixing of Ti-PILC and the V solution, and the drying and calcination processes) as responsible for modifying the structural order of Ti-PILC.

XRD pattern for Na-mont in Fig. 2 show their main characteristic reflections, which were preserved in all pillared samples, indicating that the structure of montmorillonite was not destroyed after Ti-exchange and V loading. In addition, the characteristic reflection of SiO_2 (quartz) at ca. 26.7º was observed in all the samples. Moreover, peaks at 2θ ≈ 25.2º, 48.3º and 53.9º display in the pillared samples spectra assigned to the anatase phase of TiO_2 [40,41]. The presence of TiO_2 suggests that after calcination of the pillared clays Ti-polycations precursors were crystallized into TiO_2 anatase between the clay layers. This result accounts for the successful formation of the pillars in Na-mont. The spectra of the V-modified samples did not show the reflections at 2θ ≈ 20.3, 26.3 and 31.2° assigned to the crystalline phase V_2O_5. The absence of these signals could be associated to particle size below the

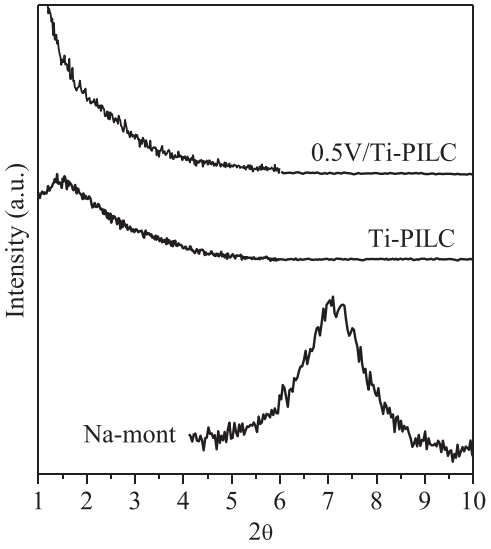

Fig. 1. Low-angle XRD patterns of: Na-mont, Ti-PILC and 0.5V/Ti-PILC.

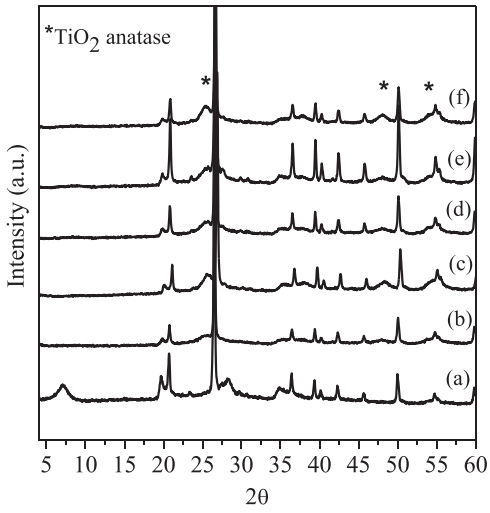

Fig. 2. XRD patterns of: (a) Na-mont, (b) Ti-PILC, (c) 0.5V/Ti-PILC, (d) 0.75V/Ti-PILC, (e) 1V/Ti-PILC, (f) 2V/Ti-PILC.

XRD detection limit (5 nm). Therefore, the result suggests that vanadium oxidic species are either in an amorphous form or highly dispersed on Ti-PILC [32,42].

Fig. 3 shows the N_2 adsorption-desorption isotherms of Ti-PILC and the V/Ti-PILC series. According to IUPAC, they can be classified as type IIb with a hysteresis loop that indicates the presence of mesopores and N_2 adsorption at low relative pressures indicates the presence of micropores [43]. The mesoporosity presented by the pillared materials could be associated with the random displacement of the clay sheets, generating delamination or a house-of-cards structure in accordance with that observed in the XRD patterns. In all samples, a hysteresis loop of the H3 type associated with the presence of slit-shaped pores is observed [32,44,45]. However, the height of the hysteresis loop decreased with the increase of V in the solids, due to the decrease in pore volume by the blockage of the pores with vanadium species [46].

Table 1 shows the results of the samples textural characterization based on the isotherms. The specific area of the pillared samples ($S_{BET} \geq 87\ m^2/g$) was higher than that of Na-mont ($31\ m^2/g$) indicating the insertion of Ti oligomers between the silicate layers of the clay, which produce its expansion. The distance between clay layers can increase by rigid pillars or by irregular laminar arrangement, in both cases greater porosity is produced. Although S_{BET} of Ti-PILC ($183\ m^2/g$) allows a good dispersion of vanadium, as the V loading increases (Table 1) the specific surface area and the micropores and mesopores volume decrease. This fact could be associated with the probable blockage of some pores by progressive filling with V species [47]. In addition, the pore size distribution of the samples was calculated with the NLDFT model for pillared clays. The results in Fig. 4A (d_p = 1–10 nm) and 4B (d_p = 10–35 nm) showed practically the same pore size distribution profiles for all samples, with presence of micropores and mesopores. All samples showed a narrow and unimodal pore diameter distribution in the micropore range around 1.5 nm (Fig. 4A) but a very broad distribution in the mesopores range with three low maxima (Fig. 4B). This broadness is coherent with the distorted structure revealed by XRD. While mesopores seemed not affected with increasing V content, micropores volume decreased, due to pore blockage by VO_x species. This blocking may explain the progressive decrease of surface area with the increase of V content (Table 1).

Diffuse Reflectance UV–vis spectroscopy (DR-UV–vis) is a suitable technique to study the coordination environment of metal ions in synthesized solids. Fig. 5 shows the DR-UV–vis spectra of the dehydrated samples. In Ti-PILC spectrum, the absorption band centered around 240 nm is assigned to the presence of isolated Ti^{4+} ions in tetrahedral coordination [33,47,48]. Although the charge transfer between the oxygen ligands and the Fe^{3+} ions present in the octahedral layer of the clay could also contribute the absorption in this region [47,49], the very low content detected by XPS results (see below) allows to exclude its influence. Bahranowski et al. [48], based on literature reports about titania/silica interface interaction [50,51], proposed that isolated Ti^{4+} ions in tetrahedral coordination species would be located between the pillar and the tetrahedral silicate layer of the clay forming the bond. Moreover, the absorption band displayed between 270 and 400 nm with a maximum around 320 nm indicates the presence of anatase phase of

Table 1
Textural characteristics and analytical V loading of synthesized samples.

Sample	S_{BET} (m^2/g)	$V_{\mu p}$ [a] (cm^3/g)	V_{mp} [b] (cm^3/g)	V loading [c] (wt%)
Ti-PILC	183	0.054	0.096	–
0.5V/Ti-PILC	132	0.025	0.128	0.42
0.75V/Ti-PILC	128	0.017	0.117	0.56
1V/Ti-PILC	94	0.015	0.108	0.87
2V/Ti-PILC	87	0.012	0.097	1.55

[a] Micropores volume obtained by the αS-plot method.
[b] Mesopores volume obtained by the αS-plot method.
[c] Determined by ICP-OES analysis.

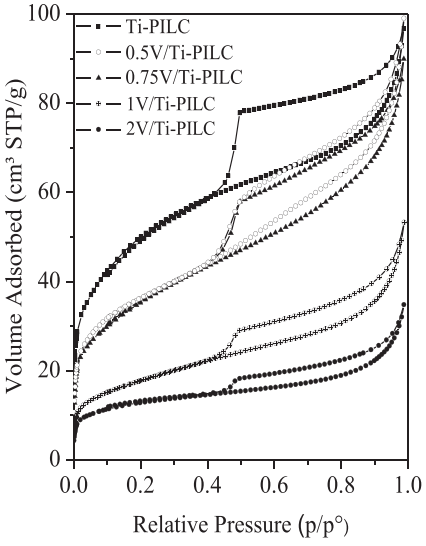

Fig. 3. N_2 adsorption/desorption isotherms of: Ti-PILC, 0.5V/Ti-PILC, 0.75V/Ti-PILC, 1V/Ti-PILC and 2V/Ti-PILC.

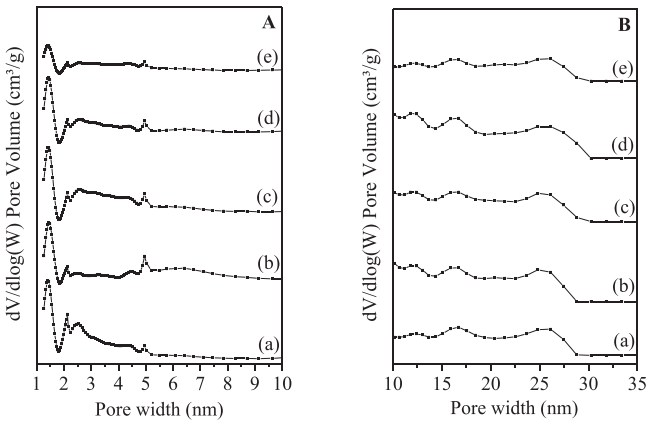

Fig. 4. Pore size distribution profiles for d_p = 1–10 nm (A) and d_p = 10–35 nm (B) of samples: (a) Ti-PILC, (b) 0.5V/Ti-PILC, (c) 0.75V/Ti-PILC, (d) 1V/Ti-PILC, (e) 2V/Ti-PILC.

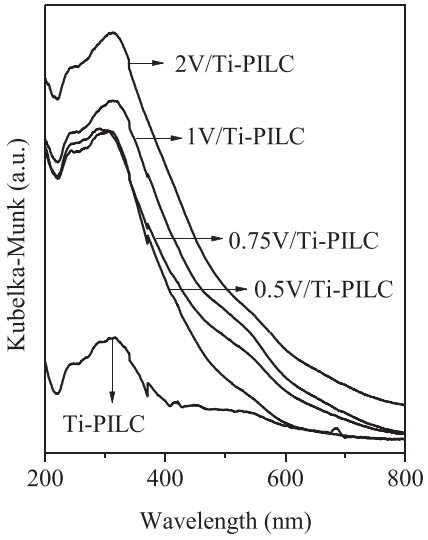

Fig. 5. DR-UV–vis spectra of the samples.

TiO_2 in this sample [48], in accordance with the phase observed in the XRD pattern.

The spectra of V-modified samples retained all the absorption bands observed in Ti-PILC with a progressive increase of the intensity in the band between 270 and 400 nm as V loading increased. The charge transfer transitions between oxygen ligands coordinated with isolated V^{5+} in tetrahedral coordination contribute the absorption in this region [52]. Additionally, a new band between 400 and 500 nm appears due to the presence of V^{5+} in oligomers with octahedral coordination. The intensity of the mentioned bands becomes more pronounced as the V loading increases, associated to the greater degree of polymerization of these species. The absorption band displays in the range 500 – 550 nm could be attributed to V_2O_5 crystallites domains [49]. This result suggests that the size of crystallites must be smaller than 5 nm as they are not detected by XRD.

Raman spectra of Ti-PILC and V/Ti-PILC samples are shown in Fig. 6. Ti-PILC spectrum shows well resolved bands around 150, 200, 399, 517, and 642 cm^{-1} assigned to anatase phase of TiO_2 [48]. These bands can be attributed to the five Raman-active modes of the anatase phase with the symmetries of Eg, Eg, B1g, A1g, and Eg, respectively [53]. According to Chen et al. [54] and Agustian et al. [55] the presence of these Raman bands indicates that TiO_2 anatase is the standard phase anchored to the Na-mont layers, which proves that the pillaring process was carried out successfully. In addition, a band well defined around 466 cm^{-1} and other with weak intensity at 708 cm^{-1} are shown in Ti-PILC spectrum and assigned at stretching vibrational modes of SiO_4 tetrahedral units [56,57]. These signals are Raman spectral features of phyllosilicates, particularly due to the lattice vibrations of dioctahedral montmorillonitic clay minerals. In addition, a band at 294 cm^{-1} appears and assigned to bending of O-H-O triangle present in the clay [58]. All the bands are preserved in V-modified samples spectra. However, their intensity decreases as the V loading increases because the V species begin to cover the surface of Ti-PILC. Furthermore, the bands corresponding to the vibrational modes of crystalline V_2O_5 (998, 706, 530, 489,410, 305, 289, 203 and 159 cm^{-1}) are not observed [52]. The absence of these bands suggests that vanadium species are dispersed well on the surface of Ti-PILC, in accordance with literature [52].

XPS analysis was used to obtain information on the surface composition of the catalysts and the chemical state of the species on the support. XPS spectra for Ti-PILC and V/Ti-PILC series are shown in Fig. 7. All samples display in their survey spectrum the characteristic signals of

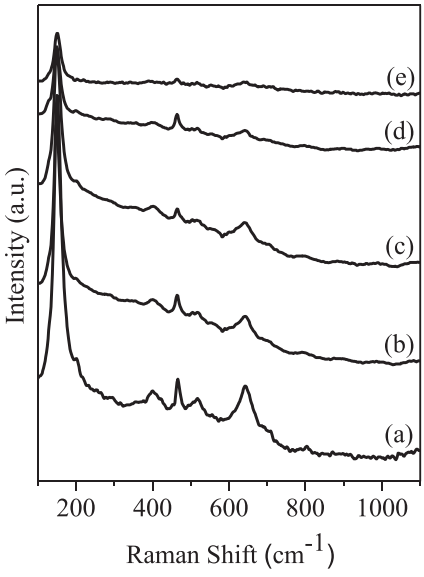

Fig. 6. Raman spectra of: (a) Ti-PILC, (b) 0.5V/Ti-PILC, (c) 0.75V/Ti-PILC, (d) 1V/Ti-PILC, (e) 2V/Ti-PILC.

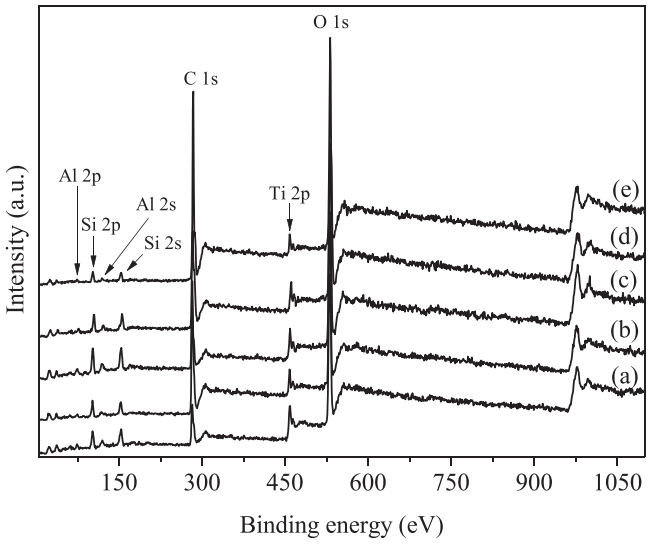

Fig. 7. XPS survey spectra of: (a) Ti-PILC, (b) 0.5V/Ti-PILC, (c) 0.75V/Ti-PILC, (d) 1V/Ti-PILC, (e) 2V/Ti-PILC.

the components present in aluminosilicate structures of clays. The signals at 74.2 eV and 120.1 eV are assigned to Al2p and 2 s, respectively; those observed at 103.1 eV and 153.7 eV to Si2p and 2 s, respectively; and the broad one centered around 531.1 eV is assigned to O1 s [59]. They also show indications of a signal ca. 710 eV, attributable to $Fe2p_{3/2}$, but too weak to be integrated. In addition, only the spectra of samples with the higher V content (>0.75 wt% V) showed indications of a signal at 168.9 eV attributable to $S2p_{3/2}$ of S^{6+} species in the form of $(SO_4)^{2-}$, remains from the V precursor used ($VOSO_4.xH_2O$). Nevertheless, their intensity was so low that it was not possible to measure them. Thus, the amount of $(SO_4)^{2-}$ was negligible compared to that of Ti and V, and its influence on the catalytic activity should be also insignificant.

The broad O1 s signal was deconvolved into two peaks due to different oxygen-containing chemical bonds (Fig. 8), with maxima at 530.3 eV and 532.5 eV. For the sake of discussion, they will be named hereinafter as species O(lbe) and O(hbe), where the acronym in brackets stands for low and high binding energy, respectively.

Assignment of these species for mixed oxides containing silica and alumina and/or titania has been matter of discussion. For silica, zeolites and sodium aluminate, Barr et al. [60] assigned the O(lbe) to Al-O bonds and the O(hbe) to Si-O bonds, and reported O1 s BE of 532.0 eV for montmorillonite, due to the apparent conversion of some of the octahedral Al to $Al(OH)_2^+$ cations. Similarly, Pawlak et al. [61] assigned the O1s BE ~532 eV to Al-O bonds in perovskites. However, Stakheev et al.

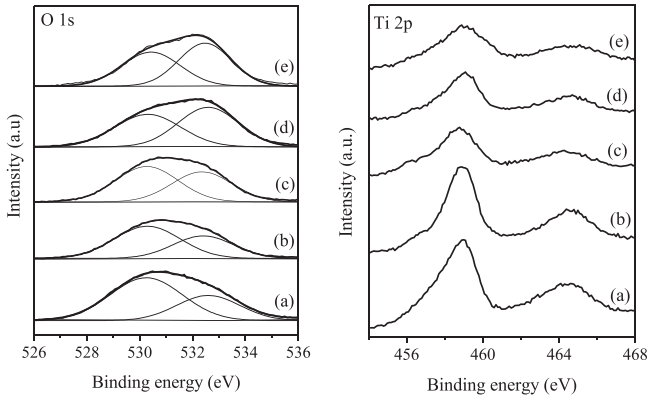

Fig. 8. XPS spectra of O1 s and Ti2p: (a) Ti-PILC, (b) 0.5V/Ti-PILC, (c) 0.75V/Ti-PILC, (d) 1V/Ti-PILC, (e) 2V/Ti-PILC.

[62] assigned such peak to Si-O bonds and the O(lbe) at 530.2 eV to Ti-O bonds. Nevertheless, Dupin et al. [63] reported a double O1s peak for TiO_2 rutile, with maxima at 530.0 (87 % and 531.8 eV (13 %).

Interestingly, for vanadium oxides with every V oxidation state between 3+ and 5+, the reported BE for the O1s peak is 529.8 – 530.5 eV [64,65]. This explains why addition of V to Ti-PILC did not modify markedly the profile of the O1 s peak.

More recently, the O(lbe) peak at 530.3 eV, labelled as O_β or O_{latt}, was attributed to the presence of lattice oxygen O^{2-} from montmorillonite and the other oxides present [40,66], while the O(hbe) at 532.5 eV, labelled as O_α or O_{ads}, was assigned to surface and chemisorbed oxygen species, which include O_2^-, O_2^{2-}, O^- and OH^- surface species on the montmorillonite, anatase and vanadium oxidic species [40,66]. The amount of oxygen species is calculated according to the relative areas of the peaks and the O(lbe)/O(hbe) atomic ratio on the surface of the samples are shown in Table 2. The results reveal that the O(lbe)/O(hbe) ratio rises as V loading on Ti-PILC increases. The chemisorbed oxygen species are often more reactive in oxidation reactions due to their higher mobility compared to lattice oxygen [67].

Additionally, Fig. 8 shows the Ti2p spectra of the samples with $Ti2p_{3/2}$ and $Ti2p_{1/2}$ signals at 458.9 eV and 464.5 eV, respectively, attributed to the presence of the anatase phase of TiO_2, and indicate 4+ oxidation state for Ti [68]. The intensity of Ti2p signal decreased when the V loading increase in the samples, indicating the increasing covering of titania by V due to the greater degree of polymerization of V species, in concordance with DR-UV–vis results [69].

The Ti and Si surface content of Ti-PILC determined by XPS analyses and the analytical Ti/Si atomic ratio are shown in Table 2. The surface Ti/Si atomic ratio is lower than value determined by ICP-OES, revealing that most of titanium remains in the interior of the mesopores due to the formation of Ti pillars in Na-mont interlayer [68].

Furthermore, $V2p_{3/2}$ XPS spectra of 1V/Ti-PILC and 2V/Ti-PILC were deconvolved into two binding energies: 516.3 and 517.5 eV, 516.2 and 517.4 eV respectively (Fig. 9). Spectra of the samples with vanadium loading $<$ 1 wt% did not exhibit a defined vanadium XPS signal, which inhibits their analysis, and are not presented in this work. The signal in the range 516.0–516.5 eV can be related to the presence of V^{4+}, while the one in the range between 517.0 and 517.7 is assigned to V^{5+} according to the literature [52,67,69,70]. The results from XPS analysis are shown in Table 3. V^{4+} and V^{5+} species coexist in both samples with a ratio V^{4+}/V^{5+} lower than 1. These results indicate the V^{4+} species present in the precursor were not totally oxidized to V^{5+} through calcination stage. Some authors reported that V^{4+} ions would induce the formation of oxygen vacancies, which generates adsorption sites for oxygen [71]. Therefore, these results agree with O_{ads}/O_{latt} ratios obtained for the materials with the highest content of V.

XPS analyses were used to determine the surface V content and V/(Ti+Si) atomic ratio (Table 3). The result revealed that V content on the surface increases directly with the V loading incorporated. Additionally, comparison of V/(Ti+Si) atomic ratios calculated from ICP-OES analysis (Table 3) demonstrate that the surface is highly enriched in V, as could be expected from the wet impregnation method used.

Table 2
XPS and ICP-OES analysis data of the samples.

Sample	O1 s binding energy (eV)		O(lbe)/O(hbe) area ratio	(Ti/Si)$_s$[a]	(Ti/Si)$_b$[b]
	O (lbe)	O (hbe)			
Ti-PILC	530.3	532.6	0.57	0.058	0.275
0.5V/Ti-PILC	530.3	532.4	0.64		
0.75V/Ti-PILC	530.3	532.4	0.81		
1V/Ti-PILC	530.3	532.5	1.11		
2V/Ti-PILC	530.4	532.5	1.14		

[a] Surface atomic ratio determined by XPS.
[b] Bulk atomic ratio determined by ICP-OES.

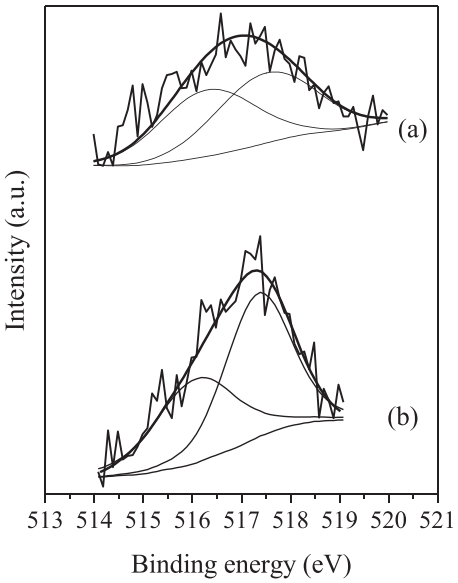

Fig. 9. $V2p_{3/2}$ XPS spectra deconvolution of: (a) 1V/Ti-PILC and (b) 2V/Ti-PILC.

Table 3
XPS and ICP-OES analysis data of 1V/Ti-PILC and 2V/Ti-PILC.

Sample	$V2p_{3/2}$ binding energy (eV)		V^{4+}/V^{5+}	(V/Ti+Si)$_s$[a]	(V/Ti+Si)$_b$[b]
	V^{4+}	V^{5+}			
1V/Ti-PILC	516.3	517.5	0.88	0.065	0.018
2V/Ti-PILC	516.3	517.5	0.74	0.139	0.034

[a] Surface atomic ratio determined by XPS.
[b] Bulk atomic ratio determined by ICP-OES.

3.2. Catalytic activity

The synthesized catalysts were evaluated in the selective oxidation of EtOH in the gas phase with O_2. The stability of the samples under reaction conditions during the testing period was determined by checking

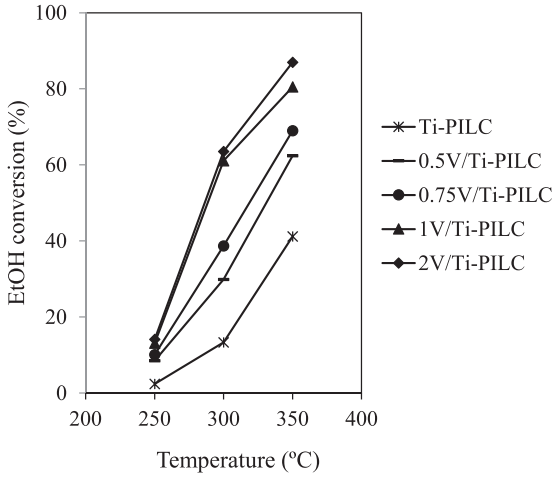

Fig. 10. Influence of temperature and V content on EtOH conversion over the synthesized catalysts. Ratio O_2/EtOH = 1 and W/F = 1.55 g_{cat}.h/mol EtOH.

reproducibility of repeated analysis in each temperature step. Fig. 10 shows EtOH conversion for all synthesized catalysts as a function of reaction temperature (T) (range 250 – 350 ºC) and V content (range 0.5–2 wt%) using a ratio of O_2/EtOH = 1 and W/F = 1.55 gcat.h/mol EtOH. As can be seen, EtOH conversion increased markedly with the increase in temperature and V content. Although Na-mont was inactive in the reaction under study, EtOH conversion over Ti-PILC was close to 40 % at 350 ºC. The catalytic activity in Ti-PILC may be associated to the presence of isolated Ti^{4+} ions, as detected by XPS, in tetrahedral coordination, as detected by DR-UV–vis, in addition to the higher specific surface and porosity available in this sample than in Na-mont. Furthermore, the results indicated that vanadium is active in EtOH oxidation, as it greatly increases their conversion. Thus, the catalytic activity of Ti-PILC for EtOH oxidation reached the highest value of EtOH conversion (87 %) over 2V/Ti-PILC at 350 °C.

Acetaldehyde (AcH) was the main product of EtOH oxidation on each catalyst in the whole temperature range evaluated, reaching AcH selectivity values between 83 % and 90 % as shown in Fig. 11. As can be seen, AcH selectivity of 85 % is reached for the highest EtOH conversion (87 %) over 2V/Ti-PILC at 350 ºC. In addition, minor products were obtained such as acetic acid, ethene, carbon oxides, ethers and others. The distribution of their selectivity as a function of the EtOH conversion for all catalysts in the temperature range explored is shown in Fig. 12. Acetic acid selectivity remained below 2 % and ethene selectivity did not exceed 5 % under the conditions evaluated. According to literature [12,13], AcH formation over catalysts proceeds through the oxidative dehydrogenation of EtOH. Acetic acid formation should occur as a consecutive oxidation of the initially formed AcH. Furthermore, the dehydration of alcohols is a characteristic reaction of the acid sites of transition metal oxides [72]. Thus, the formation of small amounts of ethene could indicate the presence of a smaller amount of these sites in the catalysts evaluated.

Both carbon oxides were produced on every catalyst by AcH oxidation, their selectivity increasing with the EtOH conversion and reaction temperature. The formation of carbon oxides was greater for catalysts with a V content above 0.75 wt%, causing AcH selectivity to decrease more significantly over these samples at higher temperatures due to its transformation to carbon oxides. Nevertheless, CO_x selectivity did not exceed 7 % on the synthesized catalysts.

To evaluate the effects of V loading in EtOH conversion, the V surface density was employed as a parameter to examine the dispersion of this metal on the catalyst surface [45]. This parameter, defined as the number of vanadium atoms per square nanometer of the catalyst surface, is a ratio between the V content and S_{BET}. Fig. 13 shows the influence of V surface density on the EtOH conversion under the conditions studied. Both the dispersion of the V and the reaction temperature influence the conversion of EtOH. At 250 ºC EtOH conversion increased little with increasing V surface density. Instead, EtOH conversion grew markedly when V surface density increased up to 1V atom/nm^2 at 300 and 350 ºC. A further increase in V content on the catalyst surface did not produce a significant increase in EtOH conversion at both temperatures. This indicates that the nature of the oxidic vanadium species (isolated, polymeric or three-dimensional particle) influence of the dispersion of the metal on the catalyst surface. From the significant EtOH conversion increase with the increase of V content up to 1 wt% it can be inferred that the catalytic activity of these catalysts is related to the dispersion and high intrinsic activity of the isolated tetrahedral V sites detected by UV–vis-DR spectra and XRD patterns. The number of the accessible vanadium centers and the majority of isolated vanadium centers in these catalysts are relevant in this reaction. However, a subsequent addition of V does not produce significant changes in the EtOH conversion at 250 and 300 ºC, there is only an slight increase at 350 ºC until reaching the maximum EtOH conversion of 87 %. This result agrees with the greater degree of polymerization of the V species in 2V/Ti-PILC catalyst (Fig. 5). So, when doubling the V load from 1 to 2 wt%, most of the additional V atoms may be not accessible, which might explain that alcohol conversion did not increase in accordance to the increase of V content.

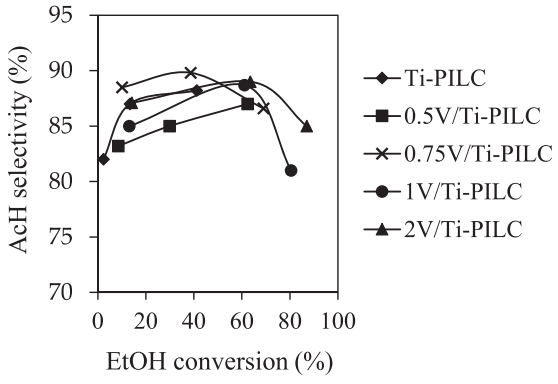

Fig. 11. AcH selectivity as a function of EtOH conversion for the synthesized catalysts in temperature range explored. Ratio: O_2/EtOH = 1 and W/F = 1.55 gcat.h/mol EtOH.

The most active catalyst, 2V/Ti-PILC, was selected to investigate the effect of oxygen concentration in the feed on EtOH conversion and AcH selectivity, by means of additional catalytic tests at 300 and 350 °C (Fig. 14). At 300 ºC, increasing oxygen content from O_2/EtOH = 0.5 (stoichiometric value) to 1.5 increased EtOH conversion by ca 10 % while AcH selectivity remained almost constant, reaching values of 66 % and 90 %, respectively, for O_2/EtOH = 1.5. At a variance, at 350 ºC EtOH conversion was increased when O_2/EtOH increased from 0.5 to 1, without further change with a subsequent increase in the O_2 concentration. However, AcH selectivity decreased with any increase of the oxygen concentration increase because it promoted the formation of CO_2, CO and ethene. Therefore, the maximum EtOH conversion (87 %) was reached at 350 ºC with a selectivity to AcH around 85 %, using the ratio O_2/EtOH = 1.

As our objective is to find more sustainable alternatives to get high surface area supports for vanadium catalysts, we have compared the AcH yield and selectivity values reached in our study with those reported in literature with similar and related catalysts in Table 4, to assess the relative efficiency of our catalysts.

At 250 ºC, catalyst 2V/Ti-PILC was more active that V/SBA-15 with similar vanadium load prepared by incipient wetness impregnation method [18] showing similar conversion with much lower catalyst amount, while AcH selectivity and yield was similar for near equal conversion. It was also much more active that V/HTC prepared by the same method with almost fourfold V load, showing better AcH selectivity. Comparison with the performance of the best catalyst supported on TiO_2-covered silica (V/2.0TiSi [12]) is difficult due to the much different contact time (W/F) and, hence, EtOH conversion values reached. Nevertheless, it noticeable that selectivity to AcH at ca. 90 % EtOH conversion (though in different reaction temperatures) was much higher on 2V/Ti-PILC, due to the high formation of acetic acid on V/2.0TiSi.

Performance of 2V/Ti-PILC at 350º C also surpassed that of V/SBA-15 catalysts with similar vanadium load prepared by hydrothermal and sol-gel methods [21], giving higher activity and much higher AcH selectivity. This is mostly due to the important formation of ethene over these latter, indicating that the acidic character of these SBA-15 supports affects the activity and selectivity to AcH [18]. Finally, comparison of results at 350 ºC for catalysts V/0.6TiSi and V/1.5TiSi, supported on TiO_2-covered silica, with those of 2V/Ti-PILC, shows the higher activity of this latter, and much higher AcH selectivity at similar conversions (due to higher formation of carbon oxides on the former). This leads to 2V/Ti-PILC to show the highest aldehyde yield, with reasonably high selectivity, among these similar catalytic systems. This result supports the feasibility to prepare highly performant supported vanadium

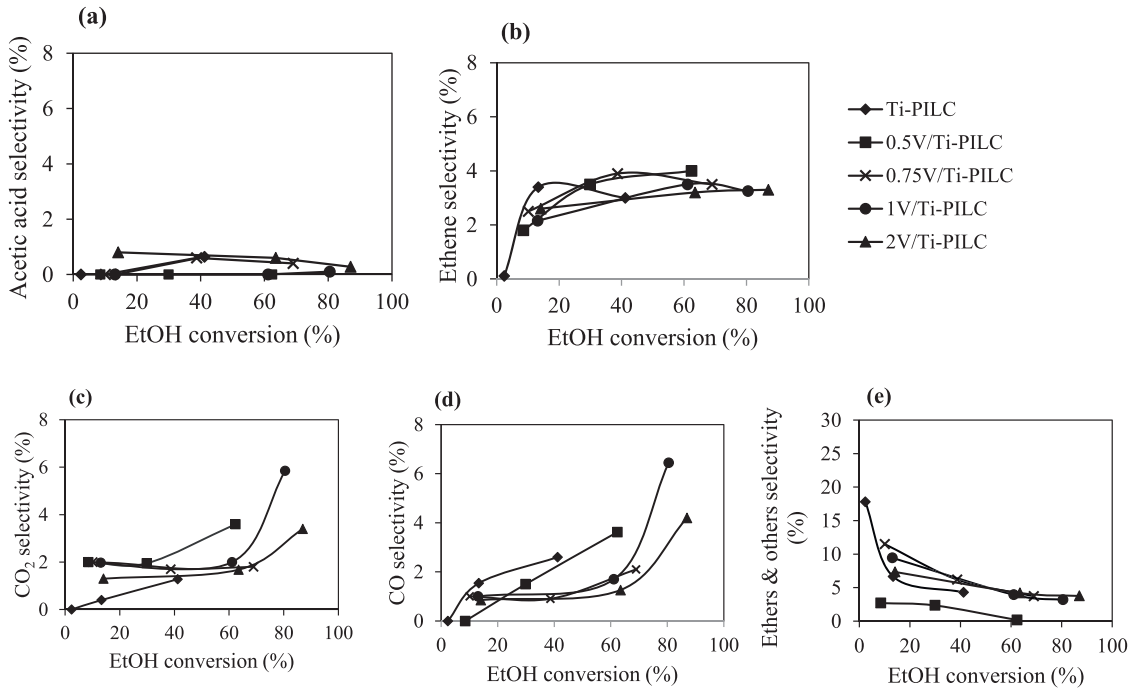

Fig. 12. Minor products selectivity as a function of EtOH conversion for the synthesized catalysts in temperature range explored. (a) Acetic acid, (b) Ethene, (c) CO_2, (d) CO, (e) Ethers & others. Ratio O_2/EtOH = 1 and W/F = 1.55 gcat.h/mol EtOH.

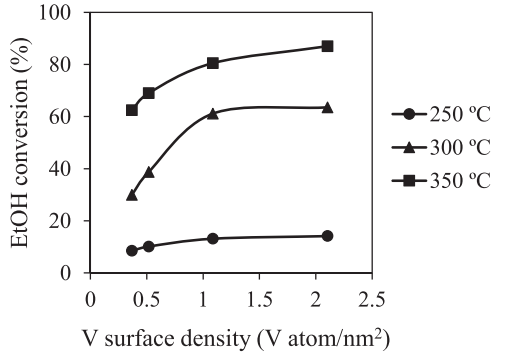

Fig. 13. Influence of V surface density on the EtOH conversion at different temperatures. Ratio O_2/EtOH = 1 and W/F = 1.55 gcat.h/mol EtOH.

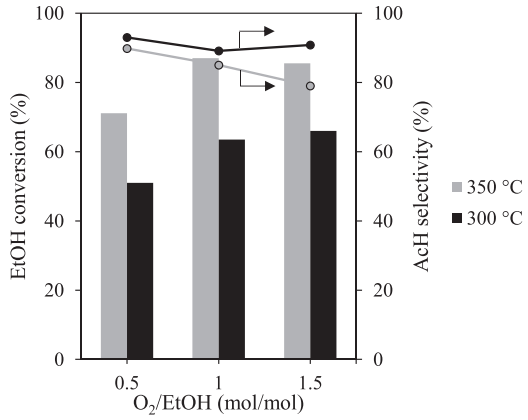

Fig. 14. EtOH conversion (columns) and AcH selectivity (lines) over 2V/Ti-PILC vs. feed composition at 300 and 350 ºC and W/F = 1.55 gcat.h/mol EtOH.

catalysts in a more sustainable way using natural clays, mild synthesis conditions and producing lesser wastes.

4. Conclusions

Based on its abundance in nature and low cost, natural clays were investigated as alternate, more sustainable raw material for supported vanadium catalysts. Montmorillonite, extracted from an Argentinian bentonite, was modified by the pillaring process with Ti to increase its specific area, porosity and interaction with the supported active species. Four low content vanadium catalysts (0.5–2 wt% V) were synthesized using the resulting Ti-PILCs as supports. Upon calcination the catalysts lost the laminar regularity but kept high micro- and mesoporosity and relatively high surface areas. The synthesized catalysts were active in EtOH oxidation with O_2 in the gas phase, with high selectivity to acetaldehyde (> 80 %) in all cases, due to the low formation of acetic acid, ethene and carbon oxides byproducts. The dispersion and structure of the V species influence the activity. Ethanol conversion increased with V loading up to 1 wt%, which is attributed to the increase of V surface density increases and the presence of isolated tetrahedral vanadium centers. A further increase of V load up to 2 wt% caused only minor improvement of activity, due to the increased degree of polymerization of these V species, which limits the activity of these materials. Though the highest acetaldehyde selectivity was observed at 300 ºC, the best acetaldehyde yield (74 %) was obtained at 350 ºC using 2V/Ti-PILC and ratio O_2/EtOH =1, with 87 % conversion and 85 % selectivity. The results of this study compare favorably with previously reported for similar ordered mesoporous vanadium catalysts. This supports the possibility of using natural clays as raw materials for catalysts for the selective aerobic oxidation of ethanol, though further studies are needed to optimize the catalysts composition and reaction conditions.

CRediT authorship contribution statement

Analía L. Cánepa: Writing – review & editing, Writing – original draft, Supervision, Project administration, Methodology, Investigation, Funding acquisition, Formal analysis, Data curation, Conceptualization.

Table 4
Comparison of catalytic performances of related vanadium catalysts in the selective oxidation of ethanol.

Catalysts	S_{BET} (m^2/g)	V load (wt%)	O_2/EtOH	T (ºC)	W/F[a]	EtOH conv. (%)	AcH	
							Select. (%)	Yield (%)
$V_2O_5/TiO_2/SiO_2$ [12]								
V/0.6TiSi	85	2.0[b]	20	350	45	85	45	38
V/1.5TiSi	128	4.6[b]	20	350	45	93	23	21
V/2.0TiSi	130	4.8[b]	20	250	45	95	51	48
V/MCM-41 [20]								
V-TIE(0.5 %)	1115	0.48	0.5	350	1.55	55	90	50
V-TIE(1 %)	1080	0.87	0.5	350	1.55	35	71	25
V/SBA-15-HT [21]	528	2[c]	0.5	350	2	56	32	18
V/SBA-15-SG [21]	512	2[c]	0.5	350	2	12	55	7
V/SBA-15 [18]	399	2.1	0.5	250	20.3	17	80	14
V/HTC [18]	122	5.6	0.5	250	20.3	12	66	8
2V/Ti-PILC[d]	87	1.55	1	250	1.55	14	87	12
2V/Ti-PILC[d]	87	1.55	1	350	1.55	87	85	74

[a] g cat.h/mol EtOH.
[b] Atom % determined by ICP-OES.
[c] Nominal V load.
[d] This work.

Sandra G. Casuscelli: Writing – review & editing, Writing – original draft, Supervision, Project administration, Investigation, Funding acquisition, Formal analysis, Data curation, Conceptualization. **Ema V. Sabre:** Writing – review & editing, Writing – original draft, Visualization, Methodology, Investigation, Formal analysis, Data curation, Conceptualization. **Vicente Cortés Corberán:** Writing – review & editing, Writing – original draft, Supervision, Resources, Methodology, Investigation, Funding acquisition, Formal analysis, Conceptualization.

Declaration of Competing Interest

The authors declare that they have no known competing financial interests or personal relationships that could have appeared to influence the work reported in this paper.

Data availability

Data will be made available on request.

Acknowledgments

The authors would like to thank Ministry of Education of Argentina Project PICT 2019-00594, UTN-FRC and CONICET (Argentina), Fundación Carolina (Spain) and Spanish Ministry of Science and Innovation (MICINN) Project PID2021-128915NB-I00 for their financial support, Prof. P. Amorós (ICMUV, Valencia University) for useful discussions and the personnel of Support Unit of ICP (CSIC) for its technical support.

References

[1] R. Sheldon, J. Kochi, Activation of Molecular Oxygen by Metal complexes. Chapter 4, in: R. Sheldon, J. Kochi (Eds.), Metal-Catalyzed Oxidations of Organic Compounds, first ed., Academic Press, New York, NY, USA, 1981, pp. 71–119. ISBN 9780126393804.
[2] T. Mallat, A. Baiker, Oxidation of alcohols with molecular oxygen on solid catalysts, Chem. Rev. 104 (2004) 3037–3058, https://doi.org/10.1021/cr0200116.
[3] H. Goksu, F. Sen, Handy and highly efficient oxidation of benzylic alcohols to the benzaldehyde derivatives using heterogeneous Pd/AlO(OH) nanoparticles in solvent-free conditions, Sci. Rep. 10 (2020) 5731, https://doi.org/10.1038/S41598-020-62695-4.
[4] M.N. Kopylovich, A.P.C. Ribeiro, E.C.B.A. Alegria, N.M.R. Martins, L.M.D.R. S. Martins, A.J.L. Pombeiro, Chapter three - catalytic oxidation of alcohols: recent advances, Adv. Organomet. Chem. 63 (2015) 91–174, https://doi.org/10.1016/bs.adomc.2015.02.004.
[5] J.C. Escobar, E.S. Lora, O.J. Venturini, E.E. Yanez, E.F. Castillo, O. Almazan, Biofuels: environment, technology and food security, Renew. Sustain. Energy Rev. 13 (2009) 1275–1287, https://doi.org/10.1016/j.rser.2008.08.014.
[6] A. Ausavasukhi, N. Krukrathok, P.J. Singthaisong, Thermal transformation of copper incorporated hydrotalcite-derived oxides and their catalytic activity for ethanol dehydrogenation, J. Ind. Eng. Chem. 117 (2023) 371–385, https://doi.org/10.1016/j.jiec.2022.10.025.
[7] ChemAnalyst "Acetaldehyde Market Size, Growth, Trends & Forecast, 2032", ⟨https://www.chemanalyst.com/industry-report/acetaldehyde-market-652⟩ (accessed 25 January 2024).
[8] M.G. Clerici, M. Ricci, G. Strukul, Formation of C-O bonds by oxidation, Ch. 2, in: G.P. Chiusoli, P.M. Maitlis (Eds.), Metal-catalysis in industrial organic processes, Royal Society of Chemistry, Cambridge, 2006.
[9] M. Eckert, G. Fleischmann, R. Jira, H.M. Bolt, K. Golka. Acetaldehyde, Ullmanś Encyclopedia of Industrial Chemistry, Wiley-VCH Verlag GmbH & Co. KGaA, Weinheim (2012), Vol. 1, 191-207.
[10] E.A. Mamedov, V. Cortés Corberán, Oxidative dehydrogenation of lower paraffins on vanadium-oxide-based catalysts: the present state of art and outlooks - A Review, Appl. Catal. A: Gen. 127 (1995) 1–40, https://doi.org/10.1016/0926-860X(95)00056-9.
[11] H. Matralis, Ch Papadopoulou, Ch Kordulis, A. Aguilar Elguézabal, V. Cortés Corberán, Selective oxidation of toluene over V_2O_5/TiO_2 catalysts. Effect of vanadium loading and of molybdenum addition on the catalytic properties, Appl. Catal. A: Gen. 126 (1995) 365–380, https://doi.org/10.1016/0926-860X(95)00029-1.
[12] N.E. Quaranta, J. Soria, V. Cortés Corberán, J.L.G. Fierro, Selective oxidation of ethanol to acetaldehyde on $V_2O_5/TiO_2/SiO_2$ catalysts, J. Catal 171 (1997) 1–13, https://doi.org/10.1006/jcat.1997.1760.
[13] T.V. Andrushkevich, V.V. Kaichev, Yu.A. Chesalov, A.A. Saraev, V.I. Buktiyarov, Selective oxidation of ethanol over vanadia-based catalysts: the influence of support material and reaction mechanism, Catal. Today 279 (2017) 95–106, https://doi.org/10.1016/j.cattod.2016.04.042.
[14] P. Čičmanec, Y. Ganjkhanlou, J. Kotera, J.M. Hidalgo, Z. Tišler, R. Bulánek, The effect of vanadium content and speciation on the activity of VOx/ZrO_2 catalysts in the conversion of ethanol to acetaldehyde, Appl. Catal., A 564 (2018) 208–217, https://doi.org/10.1016/j.apcata.2018.07.040.
[15] G.C. Bond, S.F. Tahir, Vanadium oxide monolayer catalysts preparation, characterization and catalytic activity, Appl. Catal. 71 (1991) 1–31, https://doi.org/10.1016/0166-9834(91)85002-D.
[16] M.A. Vuurman, I.E. Wachs, In situ Raman spectroscopy of alumina-supported metal oxide catalysts, J. Phys. Chem. 96 (1992) 5008–5016, https://doi.org/10.1021/j100191a051.
[17] C.A. Carrero, R. Schloegl, I.E. Wachs, R. Schomaecker, Critical literature review of the kinetics for the oxidative dehydrogenation of propane over well-defined supported vanadium oxide catalysts, ACS Catal. 4 (2014) 3357–3380, https://doi.org/10.1021/cs5003417.
[18] J. Hidalgo, Z. Tišler, D. Kubička, K. Raabova, R. Bulanek, (V)/Hydrotalcite, (V)/Al_2O_3, (V)/TiO_2 and (V)/SBA-15 catalysts for the partial oxidation of ethanol to acetaldehyde, J. Mol. Catal. A: Chem. 420 (2016) 178–189, https://doi.org/10.1016/j.molcata.2016.04.024.
[19] P. Čičmanec, K. Raabová, J. Hidalgo, D. Kubička, R. Bulánek, Conversion of ethanol to acetaldehyde over VO_X-SiO_2 catalysts: the effects of support texture and vanadium speciation, React. Kinet. Mech. Catal. 121 (2017) 353–369, https://doi.org/10.1007/s11144-017-1169-z.
[20] A.L. Cánepa, V.M. Vaschetti, K.C. Pájaro, G.A. Eimer, S.G. Casuscelli, V. Cortés Corberán, Selective oxidation of ethanol on V-MCM-41 catalysts, Catal. Today 356 (2020) 464–470, https://doi.org/10.1016/j.cattod.2019.09.052.

[21] C. Autthanit, P. Praserthdam, B. Jongsomjit, Oxidative and non-oxidative dehydrogenation of ethanol to acetaldehyde over different VOx/SBA-15 catalysts. J. Environ. Chem. Eng. 6 (2018) 6516–6529, https://doi.org/10.1016/j.jece.2018.10.015.

[22] A. Gil, L.M. Gandia, M.A. Vicente, Recent advances in the synthesis and catalytic applications of pillared clays, Catal. Rev. Sci. Eng. 42 (2000) 145–212, https://doi.org/10.1081/CR-100100261.

[23] M. Naswir, S. Arita, S. Marsi, Activation of bentonite and application for reduction pH, color, organic substance, and iron (Fe) in the peat water, Sci. J. Chem. 1 (2013) 74–82, https://doi.org/10.11648/j.sjc.20130105.14.

[24] J.T. Kloprogge, Synthesis of smectites and porous pillared clay catalysts: a review, J. Porous Mater. 5 (1998) 5–41, https://doi.org/10.1023/A:1009625913781.

[25] J.L. Valverde, A. de Lucas, P. Sanchez, F. Dorado, A. Romero, Cation exchanged and im-pregnated Ti-pillared clays for selective catalytic reduction of NOx by propylene. Appl. Catal., B 43 (2003) 43–56, https://doi.org/10.1016/S0926-3373(02)00274-6.

[26] J.P. Chen, M.C. Hausladen, R.T. Yang, Delaminated Fe_2O_3-pillared clay: its preparation, characterization, and activities for selective catalytic reduction of NO by NH_3, J. Catal. 151 (1995) 135–146, https://doi.org/10.1006/jcat.1995.1016.

[27] J.R. Butruille, T.J. Pinnavaia, Propene alkylation of liquid phase biphenyl catalyzed by alumina pillared clay catalysts, Catal. Today 14 (1992) 141–154, https://doi.org/10.1016/0920-5861(92)80018-I.

[28] N. Maes, I. Heylen, P. Cool, E.F. Vansant, The relation between the synthesis of pillared clays and their resulting porosity, Appl. Clay Sci. 12 (1997) 43–60, https://doi.org/10.1016/S0169-1317(96)00036-1.

[29] T.J. Pinnavaia, M.S. Tzou, S.D. Landau, R.H. Raythatha, On the pillaring and delamination of smectite clay catalysts by polyoxo cations of aluminum, J. Mol. Catal. 27 (1984) 195–212, https://doi.org/10.1016/0304-5102(84)85080-4.

[30] M.L. Occelli, J. Lynch, J.V. Senders, TEM analysis of pillared and delaminated hectorite cat-alysts, J. Catal. 17 (1987) 557–565, https://doi.org/10.1016/0021-9517(87)90319-8.

[31] M.L. Occelli, Surface properties and cracking activity of delaminated clay catalysts, Catal. Today 2 (1988) 339–355, https://doi.org/10.1016/0920-5861(88)85014-4.

[32] K.V. Bineesh, S.Y. Kim, B.R. Jermy, D.W. Park, Synthesis, characterization and catalytic performance of vanadia-doped delaminated zirconia-pillared montmorillonite clay for the selective catalytic oxidation of hydrogen sulfide, J. Mol. Catal. A: Chem. 308 (2009) 150–158, https://doi.org/10.1016/j.molcata.2009.04.002.

[33] L. Chmielarz, Z. Piwowarska, P. Kuśtrowski, A. Węgrzyn, B. Gil, A. Kowalczyk, B. Dudek, R. Dziembaj, M. Michalik, Comparison study of titania pillared interlayered clays and porous clay heterostructures modified with copper and iron as catalysts of the DeNOx process, Appl. Clay Sci. 53 (2011) 164–173, https://doi.org/10.1016/j.clay.2010.12.009.

[34] C. Ooka, H. Yoshida, K. Suzuki, T. Hattori, Highly hydrophobic TiO_2 pillared clay for photocatalytic degradation of organic compounds in water, Microporous Mesoporous Mater. 67 (2004) 143–150, https://doi.org/10.1016/j.micromeso.2003.10.011.

[35] F. Bergaya, The meaning of surface area and porosity measurements of clays and pillared clays, J. Porous Mater. 2 (1995) 91–96, https://doi.org/10.1007/BF00486575.

[36] P. Yuan, X. Yin, H. He, D. Yang, L. Wang, J. Zhu, Investigation on the delaminated-pillared structure of TiO_2-PILC synthesized by $TiCl_4$ hydrolysis method, Microporous Mesoporous Mater. 93 (2006) 240–247, https://doi.org/10.1016/j.micromeso.2006.03.002.

[37] P. Yuan, H. He, F. Bergaya, D. Wu, Q. Zhou, J. Zhu, Synthesis and characterization of de-laminated iron-pillared clay with meso–microporous structure. Microporous Mesoporous Mater. 88 (2006) 8–15, https://doi.org/10.1016/j.micromeso.2005.08.022.

[38] T. Mandalia, M. Crespin, D. Messad, F. Bergaya, Large interlayer repeat distances observed for montmorillonites treated by mixed Al–Fe and Fe pillaring solutions, Chem. Commun. (19) (1998) 2111–2112, https://doi.org/10.1039/A803746I.

[39] N. Jagtap, V. Ramaswamy, Oxidation of aniline over titania pillared montmorillonite clays, Appl. Clay Sci. 33 (2006) 89–98, https://doi.org/10.1016/j.clay.2006.04.001.

[40] S. Zang, G. Zhang, W. Qiu, L. Song, R. Zhang, H. He, Resistance to SO_2 poisoning of V_2O_5/TiO_2-PILC catalyst for the selective catalytic reduction of NO by NH_3, Chin. J. Catal. 37 (2016) 888–897, https://doi.org/10.1016/S1872-2067(15)61083-X.

[41] Y. Li, J.R. Liu, S.Y. Jia, J.W. Guo, J. Zhuo, P. Na, TiO_2 pillared montmorillonite as a pho-toactive adsorbent of arsenic under UV irradiation. Chem. Eng. J. 191 (2012) 66–74, https://doi.org/10.1016/j.cej.2012.02.058.

[42] H. Chae, I. Nam, S. Ham, S. Hong, Characteristics of vanadia on the surface of V_2O_5/Ti-PILC catalyst for the reduction of NOx by NH_3, Appl. Catal., B 53 (2004) 117–126, https://doi.org/10.1016/j.apcatb.2004.04.018.

[43] F.M.T. Luna, J.A. Cecilia, R.M.A. Saboya, D. Barrera, K. Sapag, E. Rodríguez-Castellón, C.L. Cavalcante, Natural and modified montmorillonite clays as catalysts for synthesis of bio-lubricants, Materials 11 (2018) 1764, https://doi.org/10.3390/ma11091764.

[44] S. Zuo, M. Ding, J. Tong, L. Feng, C. Qi, Study on the preparation and characterization of a titanium-pillared clay-supported CrCe catalyst and its application to the degradation of a low concentration of chlorobenzene, Appl. Clay Sci. 105–106 (2015) 118–123, https://doi.org/10.1016/j.clay.2014.12.033.

[45] M. Thommes, K. Kaneko, A.V. Neimark, J.P. Oliver, F. Rodríguez-Reinoso, J. Rouquerol, K.S.W. Sing, Physisorption of gases, with special reference to the evaluation of surface area and pore size distribution (IUPAC Technical Report), Pure Appl. Chem. 87 (2015) 1051–1069, https://doi.org/10.1515/pac-2014-1117.

[46] K. Soni, B.S. Rana, A.K. Sinha, B. Bhaumik, M. Nandi, M. Kumar, G.M. Dhar, 3-D ordered mesoporous KIT-6 support for effective hydrodesulfurization catalysts, Appl. Catal., B 90 (2009) 55–63, https://doi.org/10.1016/j.apcatb.2009.02.010.

[47] K.V. Bineesh, D. Kim, M. Kim, D.W. Park, Selective catalytic oxidation of H_2S over V_2O_5 supported on TiO_2-pillared clay catalysts in the presence of water and ammonia, Appl. Clay Sci. 53 (2011) 204–211, https://doi.org/10.1016/j.clay.2010.12.022.

[48] K. Bahranowski, W. Włodarczyk, E. Wisła-Walsh, A. Gaweł, J. Matusik, A. Klimek, B. Gil, A. Michalik-Zym, R. Dula, R.P. Socha, E.M. Serwicka, Ti,Zr]-pillared montmorillonite – a new quality with respect to Ti- and Zr-pillared clays, Microporous Mesoporous Mater. 202 (2015) 155–164, https://doi.org/10.1016/j.micromeso.2014.09.055.

[49] J. Arfaoui, L. Khalfallah Boudali, A. Ghorbel, G. Delahay, Effect of vanadium on the be-haviour of unsulfated and sulfated Ti-pillared clay catalysts in the SCR of NO by NH_3. Catal. Today 142 (2009) 234–238, https://doi.org/10.1016/j.cattod.2008.07.032.

[50] R. Castillo, B. Koch, P. Ruiz, B. Delmon, Influence of the amount of titania on the texture and structure of titania supported on silica, J. Catal. 161 (1996) 524–529, https://doi.org/10.1006/jcat.1996.0214.

[51] G. Lasaletta, A. Fernandez, J.P. Espinos, A.R. Gonzalez-Elipe, Spectroscopic characterization of quantum-sized TiO2 supported on silica: influence of size and TiO_2-SiO_2 interface composition, J. Phys. Chem. 99 (1995) 1484–1490, https://doi.org/10.1021/j100005a019.

[52] M.D. Soriano, J.A. Cecilia, A. Natoli, J. Jiménez-Jiménez, J.M. López Nieto, E. Rodríguez-Castellón, Vanadium oxide supported on porous clay heterostructure for the partial oxidation of hydrogen sulphide to sulfur (dx), Catal. Today 254 (2015) 36–42, https://doi.org/10.1016/j.cattod.2014.12.022.

[53] J. Zhang, S. Yan, L. Fu, F. Wang, M. Yuan, G. Luo, Q. Xu, X. Wang, C. Li, Photocatalytic degradation of rhodamine B on anatase, rutile, and brookite TiO_2. Chin. J. Catal. 32 (2011) 983–991, https://doi.org/10.1016/S1872-2067(10)60222-7.

[54] H. Chen, J. Zhan, L. Man, H. Deng, H. Zhou, L. Hao, X. Zhou, High foliar retention tannic acid/Fe^{3+} functionalized Ti-pillared montmorillonite pesticide formulation with pH-responsibility and high UV stability, Appl. Surf. Sci. 620 (2023) 156838, https://doi.org/10.1016/j.apsusc.2023.156838.

[55] E. Agustian, A. Juwono, N. Rinaldi, A.A. Dwiatmoko, Pillaring of bentonite clay with Zr, Ti, and Ti/Zr by ultrasonic technique for biodiesel production, South Afr. J. Chem. Eng. 45 (2023) 228–239, https://doi.org/10.1016/j.sajce.2023.06.001.

[56] R. Frost, L. Rintoul, Lattice vibrations of montmorillonite: a FT Raman and X-ray diffraction study, Appl. Clay Sci. 11 (1996) 171–183, https://doi.org/10.1016/S0169-1317(96)00017-8.

[57] A. Wang, J. Freeman, B. Jolliff, Understanding the Raman spectral features of phyllosilicates, J. Raman Spectrosc. 46 (2015) 829–845, https://doi.org/10.1002/jrs.4680.

[58] V. Muñoz-Iglesias, M. Fernández-Sampedro, C. Gil-Lozano, L. Bonales, O. Ercilla Herrero, M. Valles González, E. Mateo-Martí, O. Prieto-Ballesteros, Characterization of NH_4-montmorillonite under conditions relevant to Ceres, Appl. Clay Sci. 209 (2021) 106137, https://doi.org/10.1016/j.clay.2021.106137.

[59] S. Balci, A. Tecimer, Physicochemical properties of vanadium impregnated Al-PILCs: effect of vanadium source, Appl. Surf. Sci. 330 (2015) 455–464, https://doi.org/10.1016/j.apsusc.2014.12.160.

[60] T.L. Barr, S. Seal, H. He, J. Klinowski, X-ray photoelectron spectroscopic studies of kaolinite and montmorillonite, Vacuum 46 (1995) 1391–1394, https://doi.org/10.1016/0042-207X(95)00159-X.

[61] D.A. Pawlak, M. Ito, M. Oku, K. Shimamura, T. Fukuda, Interpretation of XPS O (1s) in mixed oxides proved on mixed perovskite crystals, J. Phys. Chem. B. 106 (2002) 504–507, https://doi.org/10.1021/jp012040a.

[62] A.Yu Stakheev, E.S. Shpiro, J. Apijok, XPS and XAES study of TiO_2-Si O_2 mixed oxide system, J. Phys. Chem. 97 (1993) 5668–5672, doi.org/10.1021/j100123a034.

[63] J.C. Dupin, D. Gonbeau, Ph Vinatier, A. Levasseur, Systematic XPS studies of metal oxides, hydroxides and peroxides, Phys. Chem. Chem. Phys. 2 (2000) 1319–1324. DOI:10.1039/a908800h.

[64] J. Mendialdua, R. Casanova, Y. Barbaux, XPS studies of V_2O_5, V_6O_{13}, VO_2 and V_2O_3, J. Electron Spec. Rel. Phenom. 71 (1995) 249–261, https://doi.org/10.1016/0368-2048(94)02291-7.

[65] G. Silversmit, D. Depla, H. Poelman, G.B. Marin, R. De Gryse, Determination of the V2p XPS binding energies for different vanadium oxidation states (V^{5+} to V^{0+}), J. Electron Spec. Rel. Phenom. 135 (2004) 167–175, https://doi.org/10.1016/j.elspec.2004.03.004.

[66] X. Liang, F. Qi, P. Liu, G. Wei, X. Su, L. Ma, H. He, X. Lin, Y. Xi, J. Zhu, R. Zhu, Performance of Ti-pillared montmorillonite supported Fe catalysts for toluene oxidation: the effect of Fe on catalytic activity, Appl. Clay Sci. 132-133 (2016) 96–104, https://doi.org/10.1016/j.clay.2016.05.022.

[67] J. Cheng, Y. Song, Q. Ye, S. Cheng, T. Kang, H. Dai, A mechanistic investigation on the selective catalytic reduction of NO with ammonia over the V-Ce/Ti-PILC catalysts, Mol. Catal. 445 (2018) 111–123, https://doi.org/10.1016/j.mcat.2017.11.019.

[68] F. Tomul, F.T. Basoglu, H. Canbay, Determination of adsorptive and catalytic properties of copper, silver and iron contain titanium-pillared bentonite for the removal bisphenol A from aqueous solution, Appl. Surf. Sci. 360 (Part B) (2016) 579–593, https://doi.org/10.1016/j.apsusc.2015.10.228.

[69] Y. Kim, S. Ryu, Evidences for different reaction sites for dehydrogenation and dehydration of ethanol over vanadia supported on titania, Bull. Korean Chem. Soc. 40 (2019) 489–495, https://doi.org/10.1002/bkcs.11709.

[70] X. Huang, S. Zhang, H. Chen, Q. Zhong, Selective catalytic reduction of NO with NH_3 over V_2O_5 supported on TiO_2 and Al_2O_3: a comparative study, J. Mol. Struct. 1098 (2015) 12964–12970, https://doi.org/10.1016/j.molstruc.2015.05.045.
[71] X. Li, Z. Wu, Y. Zeng, J. Han, S. Zhang, Q. Zhong, Reduced TiO_2 inducing highly active V_2O_5 species for selective catalytic reduction of NO by NH_3, Chem. Phys. Lett. 750 (2020) 137494, https://doi.org/10.1016/j.cplett.2020.137494.
[72] B. Grzybowska-Swierkosz, Acidic properties of mixed transmition metal oxides, Mater. Chem. Phys. 17 (1987) 121–144, https://doi.org/10.1016/0254-0584(87)90052-6.